Available online at www.sciencedirect.com
ScienceDirect
Journal of Power Sources 171 (2007) 321–330
JOURNAL OF POWER SOURCES
www.elsevier.com/locate/jpowsour

Transient response of a proton exchange membrane fuel cell☆

Helge Weydahl[a,1], Steffen Møller-Holst[b,*], Georg Hagen[a,2], Børre Børresen[a,3]

[a] *Department of Materials Science and Engineering, NTNU, NO-7491 Trondheim, Norway*
[b] *SINTEF Materials and Chemistry, NO-7465 Trondheim, Norway*

Received 9 November 2006; received in revised form 9 June 2007; accepted 17 June 2007
Available online 23 June 2007

Abstract

The transient response of a proton exchange membrane fuel cell (PEMFC) supplied with pure hydrogen and oxygen was investigated by load step measurements assisted by electrochemical impedance spectroscopy and chronoamperometry. Using an in-house designed resistance board, the uncontrolled response in both cell voltage and current upon step changes in a resistive load was observed. The PEMFC was found to respond quickly and reproducibly to load changes. The transient PEMFC response was limited by a cathodic charge transfer process with a potential-dependent response time. For load steps to high-current densitities, a second transient process with a constant response time was observed. This transient was offset from the charge transfer transient by a temporarily stable plateau. Results from chronoamperometry indicated that the second transient could be related to a diffusion process. Transient paths were plotted in the *V–i* diagram, matching a predicted pattern with overshooting cell voltage and current during a load step.

JEL Classification: 130.080

Keywords: Proton exchange membrane fuel cells; Transient response; Dynamic behaviour

1. Introduction

Fuel cell technology may be utilised in a wide range of applications, from portable electronics to stationary power generation. For certain applications (e.g., vehicles) where the power requirement varies rapidly, the dynamic behaviour of the fuel cell is critical. If the fuel cell is sufficiently fast to supply the required power, one can cut down on the auxiliary buffer system (super-capacitors, batteries, etc.) and thereby save cost, weight and space.

The dynamic performance of proton exchange membrane fuel cells (PEMFCs) have been reported to some degree in the open literature. Dynamic processes have been studied by both experimental approaches and modelling. Most of the experimental studies consider slow processes, such as liquid water accumulation in the gas diffusion layer [1], changes in CO coverage on the anode [2] and relaxation of membrane water content [3–5]. The reported relaxation time of these processes ranges from about 1 min to several hours. Some of the faster processes that have been studied experimentally include changes in cathode gas composition upon current steps [6] and over- and undershooting currents upon voltage steps [7–9]. A few studies report the dynamic behaviour of PEMFC stacks [10–14].

Dynamic modelling approaches usually combine a steady-state electrochemical model with time-dependent mass balances [15–18]. In such approaches the modelled fuel cell response is governed by gas transport transients. Some authors also include the capacitive effect of the charge double layer in the electrochemical model, thereby providing a more realistic description of the initial fuel cell response [19–21]. Response in cell voltage or current to a load change have been simulated in several studies [15–17,19–22], while some studies address more specific processes such as the effect of ripple currents [18], dynamic behaviour of water transport and water balance in the membrane

☆ This paper was partly presented at the 2004 Joint International Meeting of The Electrochemical Society.

* Corresponding author. Tel.: +47 92 60 45 34; fax: +47 73 59 33 50.
E-mail address: Steffen.Moller-Holst@sintef.no (S. Møller-Holst).

[1] Present address: Prototech AS, P.O. Box 6034, Postterminalen, NO-5892 Bergen, Norway.

[2] This paper is dedicated to the late Prof. Georg Hagen who contributed significantly to this work before his passing October 2004.

[3] Present address: Statoil ASA, NO-7005 Trondheim, Norway.

0378-7753/$ – see front matter © 2007 Elsevier B.V. All rights reserved.
doi:10.1016/j.jpowsour.2007.06.073

[23–25], temperature transients [26,20], effect of changing humidification and temperature of reactant gases [27,12] and transport processes in the gas diffusion layer [28,29].

Some studies take a more applied approach by assessing the dynamic interaction between PEMFCs and system components such as reformers [30–32], wind turbines [33] or batteries [10], while others simulate PEMFC operation in residential houses [34,35] or automotive applications [36–41].

This literature review shows that many aspects of dynamic PEMFC behaviour have been studied, but response in the sub-second range is scarcely documented. Knowledge of fuel cell response in this time range is critical for applications where the load changes rapidly with time, and where over- or undershooting power can damage the application. Such knowledge will further provide design criteria for required buffer systems. If the PEMFC responds sufficiently fast to load changes, auxiliary buffer systems may even become obsolete.

To our best knowledge, only Van Zee and co-workers [7–9] have measured single PEMFC response with a time resolution sufficiently high to cover the time range below 1 s: they measured the effect of e.g., stoichiometry, fuel dilution and flow field design on the transient response of a single PEMFC. Their main focus was the over- and undershooting currents observed at low stoichiometry, but their results also showed that, when supplied with excess amounts of reactant gases, the PEMFC responded as fast as the electronic load that was used to control the cell voltage. This observation stresses the importance of using a load with sufficiently short switching time when measuring sub-second PEMFC response, otherwise you will only measure the dynamic behaviour of the load itself.

The aim of this study is to investigate how fast PEMFCs respond to load changes under minimal mass transport limitations and identify the processes which determine the observed response pattern. An in-house designed, passive load with short switching time was used to reveal the autonomous response of the PEMFC, undisturbed by external control loops. To minimise mass transport limitations, the PEMFC was supplied with pure oxygen in excess. This is not a realistic condition in most fuel cell applications, but simplifies the response pattern for easier interpretation. Load step measurements were assisted by electrochemical impedance spectroscopy (EIS) and chronoamperometry to identify response limiting processes.

2. Experimental

2.1. Hardware and experimental conditions

A membrane electrode assembly from W.L. Gore & Associates (PRIMEA® 5561, Pt/Ru anode 0.45 mg cm^{-2}, Pt cathode 0.4 mg cm^{-2}, 25 μm nominal membrane thickness) was sandwiched between two gas diffusion layers from E-TEK (ELAT® carbon only). The geometric electrode area was 6.25 cm^2. The membrane electrode assembly and gas diffusion layers were mounted in a fuel cell housing from ElectroChem Inc. (EFC05-01SP-REF).

The electrodes were supplied with constant gas flows of hydrogen (99.999% purity) and oxygen (99.5% purity). To avoid any effects of fuel starvation, both gases were supplied in excess so that fuel utilisation never exceeded 50%. The gases were humidified at room temperature in separate sparging bottles. The temperature of the cathode hardware was monitored by a thermocouple from Omega®. No external heating was applied, and the operating temperature was 26 ± 1 ° C during load step measurements, 29 ± 2 ° C during EIS and 32 ± 1 ° C during chronoamperometry. These temperature variations were considered too small to affect the results significantly.

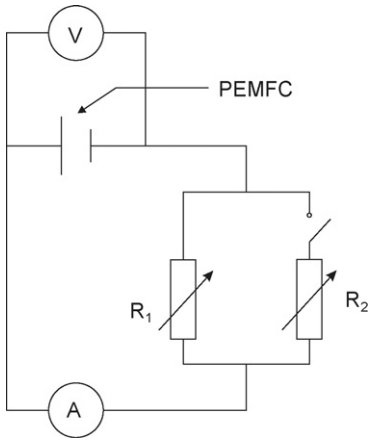

Fig. 1. Circuit diagram for the resistance step measurements.

2.2. Steps in external load resistance

Step changes in the external load resistance were obtained using an in-house designed resistance board consisting of a parallel combination of two Kool-Pak® power resistors, where one of the parallel branches was connected and disconnected using an IRF3704 MOSFET. A circuit diagram of the experimental set-up is shown in Fig. 1. When R_2 is disconnected, the external load resistance, R_L, equals R_1, and when R_2 is connected, $R_L = R_1R_2/(R_1 + R_2)$. The transistor was controlled by a 50 MHz pulse generator from Wavetek (Model 166) via an ICL7667 CPL driver circuit powered by a PULS 36 W power supply. The transistor responded by connecting or disconnecting the R_2 branch within 30 μs revealing the unregulated response in both cell voltage and current upon a step change in a purely resistive load. The resistance in each branch was selected with a switch knob, so that various external load resistances could be realised.

The unregulated response in cell voltage and current was measured with an oscilloscope from Pico Technology Ltd. (ADC-212). The current was measured with a Tektronix A6302 current probe connected to the oscilloscope via a Tektronix TM502A current probe amplifier.

2.3. Electrochemical impedance spectroscopy

EIS was carried out on the single cell described in Section 2.1 using an IM6e electrochemical workstation and PP200 add-on module from ZAHNER® elektrik. The cathode was the working electrode and the anode served as both refer-

ence and counter electrode. The ac signal had an amplitude of 5 mV and a frequency range from 100 kHz to 100 mHz. The impedance was measured at eight cell voltages (0.95, 0.90, 0.85 and 0.80–0.40 V with step intervals of 0.10 V). A complex non-linear least squares fitting program, LEVM Version 7.0, was used to fit equivalent circuit parameters to the measured impedance.

2.4. Chronoamperometry

Chronoamperometry was carried out on the single cell described in Section 2.1 with a PGSTAT20 potentiostat and BSTR 10A current booster, both from AUTOLAB®. The cathode was the working electrode while the anode served as both reference and counter electrode. During these tests, the cell voltage was kept at 0.990 V (close to the open circuit voltage) for at least 10 s before the next cell voltage was assessed. Potential steps from 0.990 V to six lower cell voltages (0.90, 0.80,. . . and 0.40 V) were investigated.

3. Theory and analysis methods

3.1. Steps in external load resistance

The fuel cell voltage is determined by the reversible voltage and the various losses in the fuel cell. These losses are typically related to ohmic resistance in the fuel cell hardware, reaction overpotentials of both anode and cathode and reactant transport limitations. The characteristics of the fuel cell response are determined by the processes involved and their corresponding relaxation times.

Typical response curves for cell voltage and current upon a step decrease in external load resistance are sketched in Fig. 2. When the external load resistance, R_L, is instantaneously reduced, the cell current instantaneously increases from I_0 to I_1. This gives an instantaneous drop in the cell voltage from V_0 to V_1 due to the ohmic resistance of the fuel cell. Ohm's law applies, giving $(V_1 - V_0)/(I_1 - I_0) = -R_\Omega$, where R_Ω is the ohmic resistance of the fuel cell.

After the ohmic drop, cell voltage relaxes towards its new steady-state value, V_2. Since the external load is purely resistive, the current relaxes towards its new steady-state value, I_2, at the same rate as the cell voltage, since $I(t) = V(t)/R_L$, according to Ohm's law.

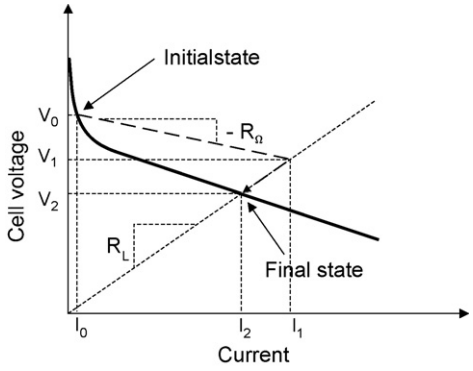

Fig. 3. Sketch of transient path (dashed line) between two steady-state operating points on the polarization curve (thick solid line) when the external load resistance is changed from a high value V_0/I_0 to a lower value $V_2/I_2 = R_L$. R_Ω is the ohmic resistance of the fuel cell. Remaining symbols are explained in Fig. 2.

As a measure of the fuel cell response time, τ_{FC} is used. This quantity is the time it takes for the cell voltage to decrease from V_1 to V_τ, where the value of V_τ is implicitly given by

$$\left|\frac{V_\tau - V_2}{V_1 - V_2}\right| = e^{-1} \tag{1}$$

where e is Euler's number. Thus, τ_{FC} corresponds to the time constant of exponential decay, even though the observed response curves were not purely exponential.

Since the switching time of the transistor was 30 μs, V_1 and I_1 were determined by linearly extrapolating the curve elements between 30 and 90 μs back to $t = 0$.

As shown in Fig. 3 the theoretical response in cell voltage and current can be plotted in the V–i diagram, showing deviation from the polarization curve, as reported previously by our group [42]. As interpreted by Zenith et al. [43], the instantaneous ohmic drop will follow a straight line with slope $-R_\Omega$ from (V_0, I_0) to (V_1, I_1), according to Ohm's law. Constant load resistance, R_L, is represented by straight lines through origo. The relaxation towards steady state from (V_1, I_1) to (V_2, I_2) will follow this line since $V(t) = R_L I(t)$. Thus (V_1, I_1) is found as the intersection between $R_L I$ and the straight line from V_0 with slope $-R_\Omega$.

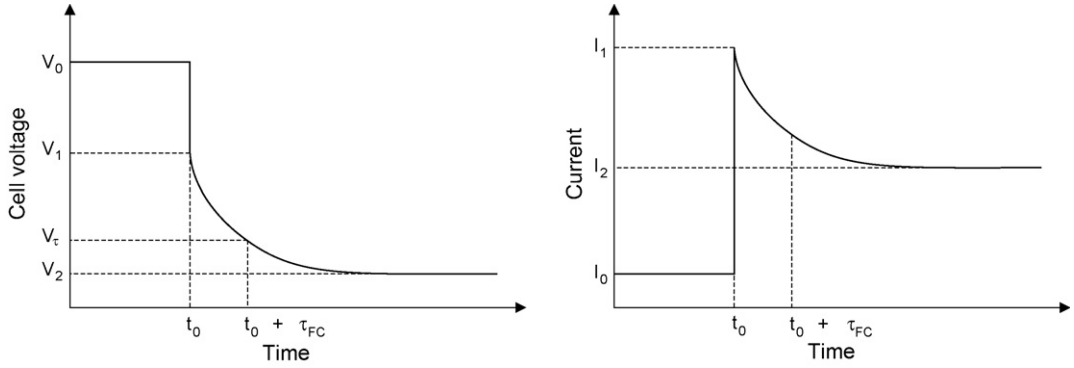

Fig. 2. Sketch of typical transient responses in cell voltage (left) and current (right) upon a step change from high to low external load resistance (not to scale).

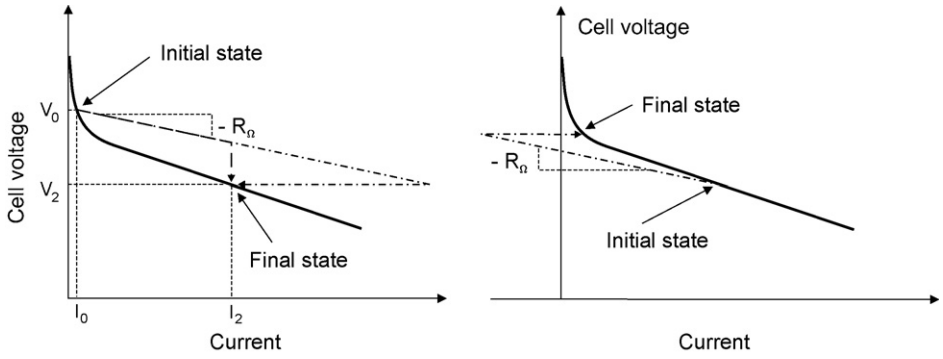

Fig. 4. (Left) Sketch of transient paths for a step in current from I_0 to I_2 (dashed line) and for a step in cell voltage from V_0 to V_2 (dash-dotted line). The steady-state polarization curve is shown as a thick solid line. (Right) Sketch of transient path for a step in cell voltage from a low to a high value, leading to temporary reversal of the current.

When controlling cell voltage or current by using a potentiostat, the transient paths will have a significantly different shape, as shown in Fig. 4. A step in current will follow a constant current path towards the new steady state, while a step in cell voltage will follow a constant voltage path (Fig. 4, left). The instantaneous ohmic drop in both cases will still follow a straight line from (V_0, I_0) with slope $-R_\Omega$. Thus, the overshoot in cell current will be much larger for a potential step than for a step in the external load resistance. This also shows that steps in cell voltage up to high cell voltages can impose a reversal of the cell current, which may cause damage to the fuel cell electrodes (Fig. 4, right).

3.2. Electrochemical impedance spectroscopy

EIS was applied to identify the processes limiting the dynamic response of the PEMFC. The equivalent circuit used to model the impedance spectra has been proposed earlier by i.e., Ciureanu and Roberge [44] and is shown in Fig. 5. The ohmic resistance between the electrodes, mainly due to the ohmic resistance in the membrane, is represented by R_Ω. The two parallel combinations of a resistance and a constant phase element (CPE) represent the charge transfer processes in the anode and cathode. CPEs are used instead of capacitances since measured impedance spectra contained depressed semi-circles, which are typical for porous electrodes [45]. Thus, R_a and R_c represent the anode and cathode charge transfer resistances, respectively, while CPE_a and CPE_c correspond to the distributed double-layer capacitance of the porous anode and cathode, respectively.

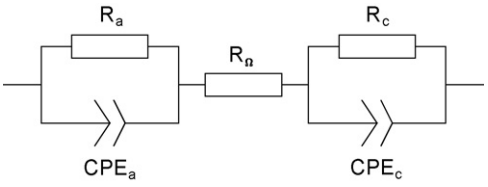

Fig. 5. Equivalent circuit for the PEMFC [44]. R_Ω is the ohmic resistance between the electrodes, R_a and R_c are the anode and cathode charge transfer resistances, respectively, and CPE_a and CPE_c are the anode and cathode CPEs, respectively.

The impedance of a CPE is [46]

$$Z_{CPE} = \frac{1}{T(i\omega)^{\phi}}, \tag{2}$$

where ω is the angular frequency, T and ϕ the CPE fitting parameters and $i = \sqrt{-1}$. The corresponding capacitance of the cathode CPE is [46]

$$C_c = [T_c(R_\Omega^{-1} + R_c^{-1})^{\phi_c - 1}]^{1/\phi_c}, \tag{3}$$

where T_c and ϕ_c are the fitting parameters of the cathode CPE. This capacitance can be used to estimate the response time of the equivalent circuit, τ_{EC}, according to

$$\tau_{EC} = R_c C_c, \tag{4}$$

where the anode contribution has been assumed negligible. Eq. (4) corresponds to the theoretical time constant of a parallel combination of a resistance and capacitance.

4. Results and discussion

4.1. Steps from high to low external load resistance

The initial response in cell voltage and current to a step decrease in the external load resistance is shown in Fig. 6. The cell voltage apparently exhibited a fast ohmic drop followed by a slower relaxation towards the new steady state. Correspondingly, the current density jumped to a higher value and then decayed towards the new steady state. In the time domain shown, there was a pronounced potential dependence of the fuel cell response: the fuel cell responded slower for steps with higher final voltages, V_2. This relaxation process is most likely due to a charge transfer process at the cathode, as will be discussed further in Section 4.3.

Fig. 7 shows steps c and d in Fig. 6 on a logarithmic time scale. For these steps, a second relaxation process appeared at appr. 0.1 s, after a temporarily stable plateau in cell voltage and current. It was verified that the external load resistance was constant during this transient, also, the same behaviour was observed using a potentiostat (see Section 4.4), so the second transient was not caused by interference from the experimental set-up. It was neither caused by insufficient supply of reactant gases, which

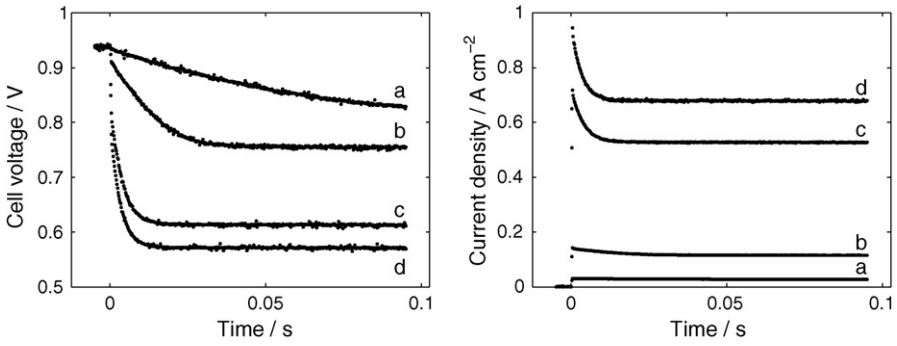

Fig. 6. First 100 ms of the transient response in cell voltage and current density upon a step change in the external load resistance from 200 Ω to (a) 5.0 Ω, (b) 1.0 Ω, (c) 0.19 Ω and (d) 0.14 Ω.

was verified by repeating the experiment with various reactant gas flow rates.

The second transient levelled out, reaching steady state within appr. 2 s for both steps c and d. Thus, the response time for this transient showed no significant dependence on current density. The voltage drop during this transient was more pronounced for step d than for step c while it was not observed for steps a and b. Apparently, a higher current density gave a larger voltage drop during the second transient. This characteristic response pattern will be further discussed in Sections 4.3 and 4.4.

Additional step measurements were carried out for varying initial and final values of the external load resistance. A selection of these steps is shown in Fig. 8. The same response pattern as described above was observed also for these steps: an immediate ohmic change in cell voltage and current followed by a slower relaxation, with a potential-dependent response time. A second transient appeared for steps with final voltages below appr. 0.65 V, reaching steady state within 2 s. Also for these steps, the voltage drop during the second transient was more pronounced for steps with lower final cell voltages. For steps with initial voltages lower than 0.53 V, the temporarily stable plateau was absent (Fig. 8f).

The ohmic resistance of the fuel cell, R_Ω, was calculated by dividing the ohmic voltage drop, $|V_2 - V_1|$, by the ohmic current step, $|I_2 - I_1|$, for all steps in Fig. 8. This gave $R_\Omega = 0.12 \pm 0.01\ \Omega\,\mathrm{cm}^2$, which is within the uncertainty limits of the value found from EIS (see Section 4.3).

To show the potential dependence of the first transient, Eq. (1) was used to calculate the corresponding response time of this part of the response curve. The response time was only calculated for the first transient; for steps where also a second transient appeared, the temporarily stable values of cell voltage and current were used as V_2 and I_2, respectively, and the further relaxation occurring after 100 ms was disregarded. For steps without temporarily stable values between the two transients, the response time was not calculated.

Fig. 9 shows the response time of the first transient for steps a–d in Fig. 8. Response times ranged from 0.38 s to 1.6 ms depending on the initial and final voltage. Steps with the same initial voltage, V_0, had a response time that decreased with lower final voltages, V_2. On the other hand, steps with the same *final* voltage had a response time that decreases with lower *initial* voltage. Thus, step size itself did not determine the response time, rather the voltage range where the fuel cell relaxed towards the new steady state.

For steps from the same initial voltage, V_0, the potential dependence of the response time was strongest for final cell voltages, V_2, above appr. 0.75 V. This corresponds to the curved activation-controlled region of the polarization curve as shown in Fig. 10. The fact that the rate-limiting process was potential dependent, suggests that it is related to charge transfer. Considering that the cathode was supplied with pure oxygen, it is not unlikely that the fuel cell response can actually be limited by charge transfer.

In Fig. 10, the response curves for steps from a high external load resistance to four lower resistances are plotted in the *V–i* diagram, exhibiting the same pattern as predicted in Section 3.1(see Fig. 3). A deviation from the predicted straight line was

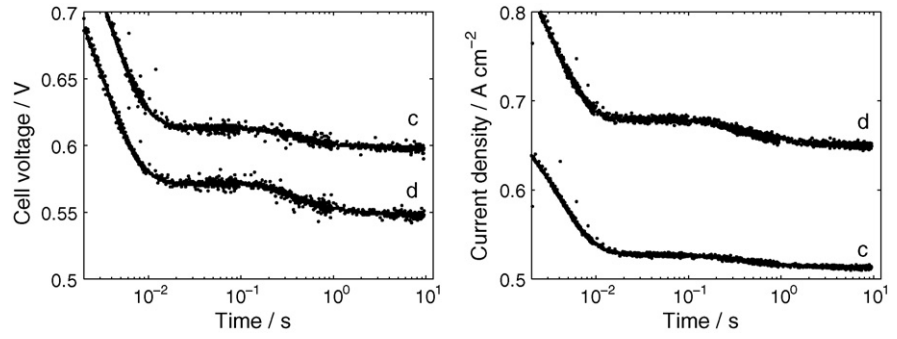

Fig. 7. Semi-logarithmic plot of steps c and d of Fig. 6 in a time interval between 2 ms and 10 s, showing the appearance of a second transient at appr. 0.1 s.

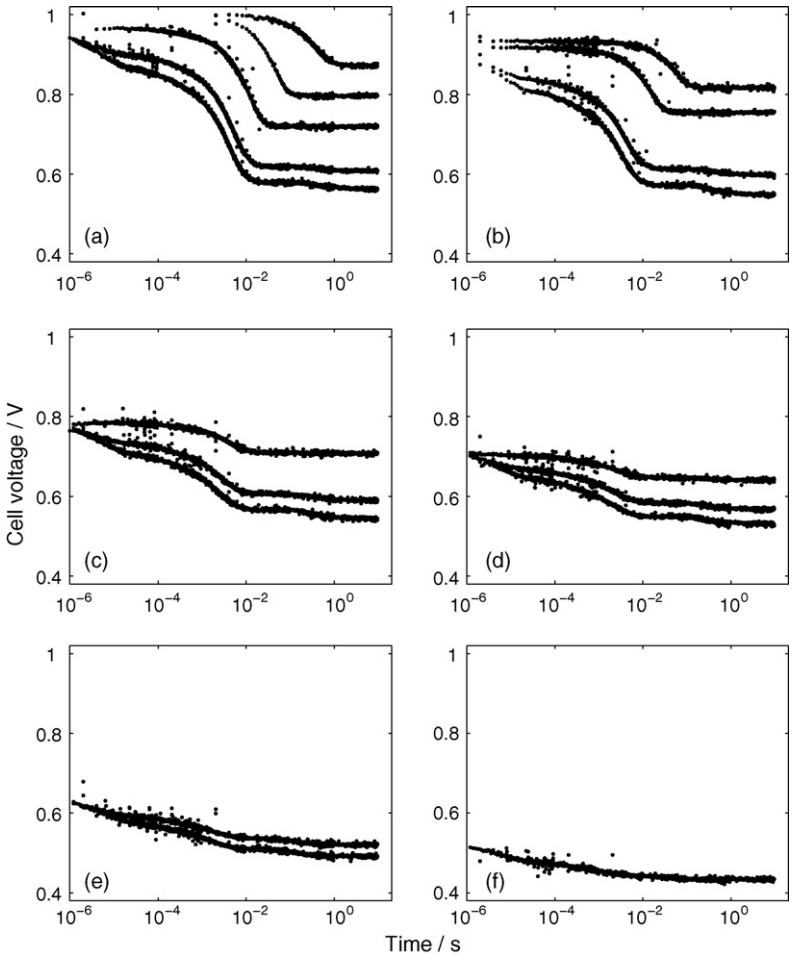

Fig. 8. Semi-logarithmic plot of response in cell voltage to step changes in the external load resistance from (a) $\infty\,\Omega$ (open circuit), (b) 200 Ω, (c) 5.0 Ω (d) 0.75 Ω (e) 0.25 Ω and (f) 0.10 Ω to lower resistance values.

observed for the first ms of the step, probably due to switching transients in the transistor and external resistances.

4.2. Steps from low to high external load resistance

Also the fuel cell response to a step increase in external load resistance was measured. Fig. 11 shows the response in cell voltage when changing the external load resistance from a low value up to 200 Ω. This corresponds to the reverse steps of those shown in Fig. 6. The response was characterised by an ohmic step in cell voltage, followed by a slower increase towards a peak value. After this peak, the cell voltage experienced a gradual

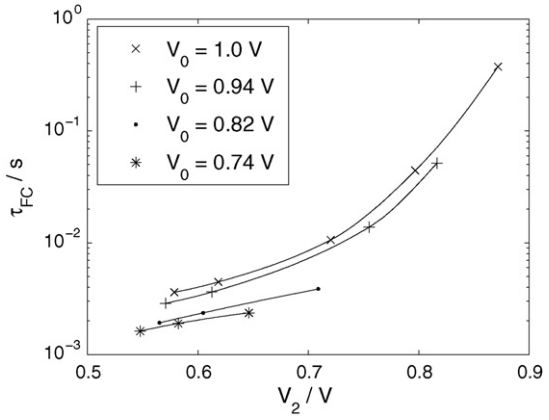

Fig. 9. Semi-logarithmic plot of the response time of steps a–d in Fig. 8 as a function of final voltage, V_2, for different initial voltages, V_0.

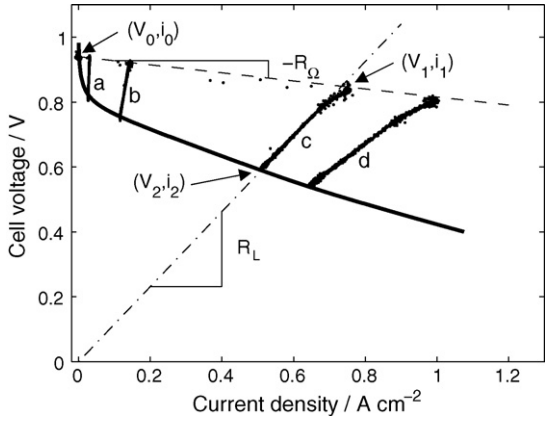

Fig. 10. Transient response (dots) plotted in the *V–i* diagram for steps in the external load resistance from 200 Ω to (a) 5.0 Ω, (b) 1.0 Ω, (c) 0.19 Ω and (d) 0.14 Ω. The dashed line has a slope of $-R_\Omega$, while the dash-dotted line has a slope of R_L corresponding to step c. The steady-state polarization curve is shown as a thick solid line.

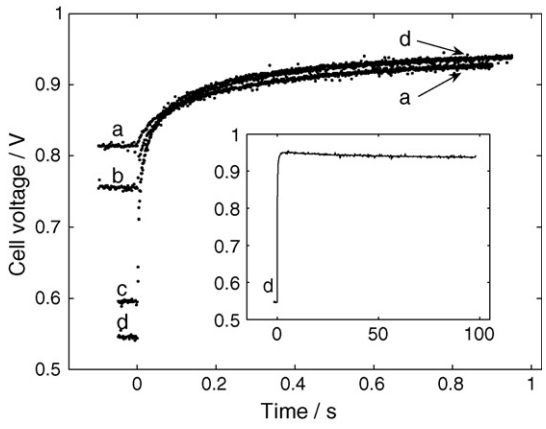

Fig. 11. The first second of the transient response in cell voltage to a step change in the external load resistance from (a) 5 Ω, (b) 1 Ω, (c) 0.15 Ω and (d) 0.10–200 Ω. (Inset) First 100 s of response curve (d).

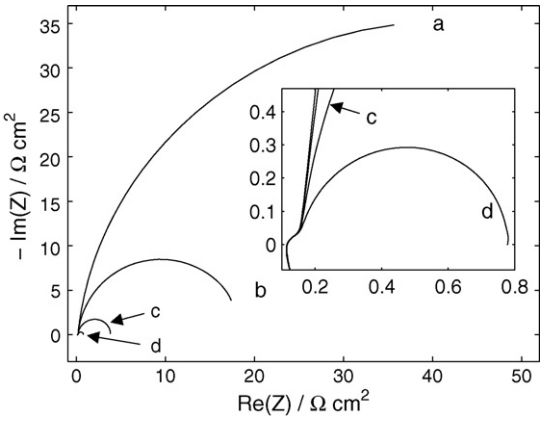

Fig. 12. Impedance spectra at (a) 0.95 V, (b) 0.90 V, (c) 0.85 V and (d) 0.80 V (hardly visible). (Inset) An expanded view of the low impedance region.

decrease, probably as oxides or other surface species formed on the cathode (Fig. 11, inset). Correspondingly, the current density (not shown) exhibited an ohmic drop, before it followed the same increase and decrease as the cell voltage, since current and voltage were related by Ohm's law. The overshoot in cell voltage was more pronounced for steps from lower cell voltages. This can be explained by removal of oxides from the electrodes at low cell voltage giving a higher cell voltage after the step. There were no significant differences in response time; all curves reached the peak value in appr. 5 s and decreased on a time scale of 100 s.

Additional steps from low to high external load resistances were studied and found to exhibit the same trend as described in the previous paragraph. The response time of these steps increased with increasing final voltage, which is in agreement with the trend for steps from high to low external load resistances, where the fuel cell was found to respond slower in regions with high cell voltages. Consequently, a step from high cell voltage to low cell voltage will take shorter time than the reverse step back to high cell voltage. For instance, the response time of a step with initial voltage 0.94 V and final voltage 0.55 V was 3 ms while the reverse step back to 0.94 V had a response time of 35 ms.

The analysis presented in this section is mainly qualitative and does not identify the processes which give rise to the observed trends. An effort to identify rate-limiting processes by standard electrochemical methods is presented in the following sections.

4.3. Electrochemical impedance spectroscopy

EIS was applied to separate and quantify the processes governing the fuel cell response. Measured impedance spectra at cell voltages between 0.95 and 0.80 V are shown in Fig. 12. Two distinct arcs were observed for each spectrum: (i) a small potential-independent arc at high frequencies (10 kHz–120 Hz) and (ii) a large potential-dependent arc at lower frequencies (120–0.1 Hz). A potential-dependent arc is normally attributed to a charge transfer process [47]. The large arcs in Fig. 12 are probably related to the charge transfer process at the cathode, since the cathode reaction in a PEMFC is known to have substantially slower kinetics than the anode reaction [48].

As the cell voltage decreased, the large arc attained the shape of a depressed semi-circle. This behaviour can be attributed to the porous structure of the electrode [45]. The inductive impedance observed at frequencies 10–100 kHz is most likely related to cables and electrical connections, and the corresponding data points were disregarded in the fitting process.

The small arc at high frequencies may be attributed to the anodic charge transfer process. The diameter of this arc was appr. 0.1 Ω cm^2 which is comparable to the anode impedance measured for a symmetric H_2/H_2 cell [49]. The arc did not change significantly with cell voltage, which is typically the case for arcs corresponding to rapid charge transfer processes.

For cell voltages 0.85 V and higher, the small high-frequency arc was almost negligible compared to the large arc. This caused unprecise fitting of the parameters corresponding to the small arc. Since the shape of this arc did not change significantly for cell voltages 0.80 V and higher, fitting parameters for this arc were kept constant above 0.80 V, using the parameter values found at 0.80 V.

For cell voltages 0.70 V and lower, the large arc still decreased with decreasing cell voltage while the small high-frequency arc remained unchanged as shown in Fig. 13. In addition, a third arc

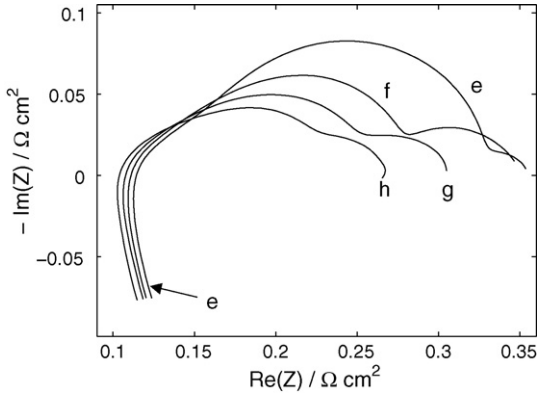

Fig. 13. Impedance spectra at (e) 0.70 V, (f) 0.60 V, (g) 0.50 V and (h) 0.40 V.

Table 1
Cathode parameters obtained from fitting of the impedance spectra at different cell voltages

Cell voltage (V)	R_c (Ω cm^2)	T_c (F cm^{-2} s$^{\phi-1}$)	ϕ_c	C_c (F cm^{-2})	τ_{EC} (s)
0.95	77.9	0.0218	0.928	0.0137	1.1
0.90	18.4	0.0203	0.952	0.0150	0.28
0.85	3.67	0.0195	0.970	0.0161	0.059
0.80	0.614	0.0210	0.967	0.0170	0.010
0.70	0.173	0.0266	0.939	0.0177	0.0031
0.60	0.151	0.0401	0.843	0.0132	0.0020
0.50	0.143	0.0650	0.757	0.0111	0.0016
0.40	0.128	0.0947	0.709	0.0111	0.0014

was observed, emerging at frequencies ranging from 3 Hz for curve e to 11 Hz for curve h. Since there was no clear trend in these arcs, no effort was made to include elements in the equivalent circuit to model this behaviour (ref. Fig. 5), and the data points corresponding to these arcs were disregarded in the fitting process. However, it is not unlikely that they correspond to the second transient reported in Section 4.1. The onset of the second transient occurred around 0.1 s, which corresponds to a frequency of 10 Hz. This is in the same range as the frequencies where the third arcs emerged. In addition, the third arc only appeared at cell voltages where also the second transient appeared.

The high-frequency crossing of the real axis decreased slightly for cell voltages decreasing from 0.70 to 0.40 V (Fig. 13). This can be explained by an increased water production on the cathode at higher currents, giving a more humidified membrane with higher conductance.

The equivalent circuit in Fig. 5 gave an excellent fit to the impedance data, as can be expected when using CPEs. The cathode parameters are shown in Table 1. The increasing cathode arc size at higher cell voltages was reflected in an increasing value for the cathode charge transfer resistance, R_c. The fitted values of ϕ_c were less than 1, which reflects the porous structure of the electrode. For cell voltages below 0.70 V, the value of ϕ_c decreased with decreasing cell voltage. This is reasonable since an increased current density will give even more inhomogeneous conditions throughout the electrode. A fitted value of R_Ω (0.11 $\pm$ 0.01 Ω cm^2) was in agreement with the value found from step measurements (see Section 3.1). The parameter values of R_Ω, R_c and C_c found here have the same order of magnitude as reported in similar studies [50,44,51].

The EIS-derived response time, τ_{EC} calculated from Eq. (4) for each cell voltage is included in Table 1. This response time had the same potential dependence and order of magnitude as τ_{FC} calculated in Section 4.1. This indicates that the large arc of the impedance spectrum is the frequency domain representation of the potential-dependent response observed in Section 4.1.

A semi-logarithmic plot of *IR*-corrected cell voltage versus R_c^{-1} (ref. Fig. 5) is shown in Fig. 14. The slope of this curve was identical to the Tafel slope found from steady-state polarization data. This confirms that R_c indeed corresponds to a charge transfer resistance [52].

In summary, results from EIS suggested that the potential-dependent response observed in Section 4.1 is related to a charge transfer process on the cathode, and that this process limits the fuel cell response at cell voltages above 0.7 V.

4.4. Chronoamperometry

Chronoamperometry was applied to assess the second transient (see Fig. 7). Step changes in cell voltage from open circuit to lower cell voltages were applied. A second transient in current after a temporarily stable plateau emerged at appr. 0.1 s for steps down to 0.60 V and lower. This is the same behaviour as observed for steps in external load resistance (ref. Fig. 7). Fig. shows a plot of current density as a function of the inverse square root of time. The curves formed straight lines after appr. 0.15 s. Solving Fick's second law of diffusion for several electrode geometries (planar, spherical, hemispherical) results in expressions where the current density is proportional to the inverse square root of time if the mass transfer of the reactants or products is controlled by diffusion [53]. Thus, the straight lines in Fig. were taken as an indication that the second transient is related to a diffusion process, even though the investigated system does not correspond to any of the ideal electrode geometries. However, the electrode might be considered as a three-dimensional array of spherical or hemispherical microelectrodes if it is assumed that the carbon is inert and all electrochemical processes take place at the catalyst particles. Consequently, even if the electrode is neither an ideal planar electrode nor a microelectrode, the observed linear

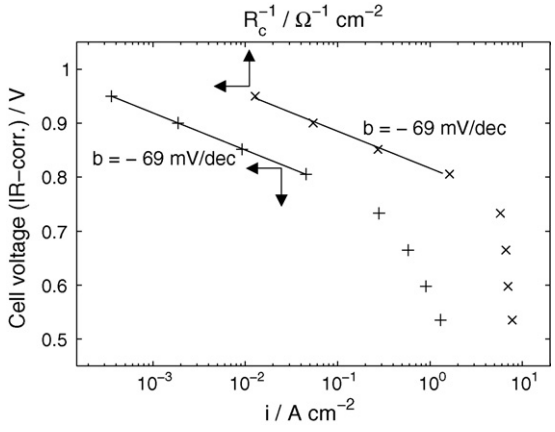

Fig. 14. Comparison of the Tafel plot generated from the polarization curve (+) and from R_c^{-1} (x), relating the potential-dependent arc to a charge transfer process.

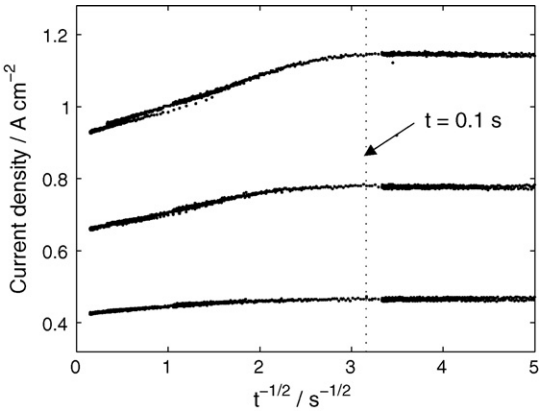

Fig. 15. Chronoamperometric measurements for potential steps from 0.990 V (close to open circuit potential) down to 0.40 V (upper curve), 0.50 V (middle curve) and 0.60 V (bottom curve). The time window from 40 ms to 45 s is shown.

relationship between current density and $t^{-1/2}$ were taken as an indication that the second transient is caused by mass transfer controlled by diffusion.

5. Conclusion

The transient response of a single PEMFC supplied with pure hydrogen and oxygen was investigated by resistance step measurements assisted by EIS and chronoamperometry. The PEMFC was found to respond quickly and reproducibly to load changes and showed excellent load-following performance.

A characteristic response pattern was identified: for steps to a lower external load resistance, an ohmic drop in cell voltage (and an equivalent ohmic step in current) was followed by a slower transient related to a charge transfer process in the cathode. Since the load was purely resistive, cell voltage and current were related by Ohm's law during the slower transient. The response time of the charge transfer transient depended on cell voltage and decreased with initial and final cell voltages. Response times in the range from 0.38 s to 1.6 ms were observed, depending on the initial and final voltages. The voltage dependence was most pronounced in the activation-controlled region of the polarization curve (0.75 V and higher). For steps with final voltages below appr. 0.65 V, a second relaxation process appeared at about 0.1 s, after a temporarily stable plateau in cell voltage and current. This relaxation process had an apparently constant response time of appr. 2 s, and chronoamperometric measurements indicated that it could be related to diffusion. Transient paths from one steady state on the polarization curve to another were shown, matching a predicted pattern. This pattern also predicted the overshoot or undershoot in cell voltage and current during the transient.

Acknowledgement

The Research Council of Norway and Aker Kværner Power & Automation Systems AS are kindly acknowledged for financial support.

References

[1] W. He, G. Lin, T.V. Nguyen, AIChE J. 49 (12) (2003) 3221–3228.
[2] K.K. Bhatia, C.-Y. Wang, Electrochim. Acta 49 (2004) 2333–2341.
[3] J.F. Moxley, S. Tulyani, J.B. Benziger, Chem. Eng. Sci. 58 (2003) 4705–4708.
[4] J. Benziger, E. Chia, J.F. Moxley, I.G. Kevrekidis, Chem. Eng. Sci. 60 (2005) 1743–1759.
[5] T. Abe, H. Shima, K. Watanabe, Y. Ito, J. Electrochem. Soc. 151 (1) (2004) A101–A105.
[6] Q. Dong, J. Kull, M.M. Mench, J. Power Sources 139 (2005) 106–114.
[7] S. Kim, S. Shimpalee, J.W. Van Zee, J. Power Sources 135 (2004) 110–121.
[8] S. Kim, S. Shimpalee, J.W. Van Zee, J. Power Sources 137 (2004) 43–52.
[9] S. Kim, S. Shimpalee, J.W. Van Zee, J. Electrochem. Soc. 152 (6) (2005) A1265–A1271.
[10] J.C. Amphlett, E.H. de Oliveira, R.F. Mann, P.R. Roberge, A. Rodrigues, J.P. Salvador, J. Power Sources 65 (1997) 173–178.
[11] S.O. Morner, S.A. Klein, J. Solar Energy Eng. 123 (2001) 225–231.
[12] W. Friede, S. Raël, B. Davat, IEEE Trans. Power Electron. 19 (5) (2004) 1234–1241.
[13] J. Hamelin, K. Agbossou, A. Laperrière, F. Laurencelle, T.K. Bose, Int. J. Hydrogen Energy 26 (2001) 625–629.
[14] W.H. Zhu, R.U. Payne, D.R. Cahela, B.J. Tatarchuk, J. Power Sources 128 (2004) 231–238.
[15] J.M. Corrêa, F.A. Farret, L.N. Canha, in: Proceedings of The 27th Annual Conference of The IEEE. Industrial Electronics Society, IECON'01, vol., 2001, pp. 141–146.
[16] S. Yerramalla, A. Davari, A. Feliachi, T. Biswas, J. Power Sources 124 (2003) 104–113.
[17] L.-Y. Chiu, B. Diong, R.S. Gemmen, IEEE Trans. Ind. Appl. 40 (4) (2004) 970–977.
[18] R.S. Gemmen, J. Fluids Eng. 125 (2003) 576–585.
[19] M. Ceraolo, C. Miulli, A. Pozio, J. Power Sources 113 (2003) 131–144.
[20] X. Xue, J. Tang, A. Smirnova, R. England, N. Sammes, J. Power Sources 133 (2004) 188–204.
[21] P.R. Pathapati, X. Xue, J. Tang, Renew. Energy 30 (2005) 1–22.
[22] S. Um, C. Wang, K. Chen, J. Electrochem. Soc. 147 (12) (2000) 4485–4493.
[23] F. Chen, Y. Su, C. Soong, W. Yan, H. Chu, J. Electroanal. Chem. 566 (2004) 85–93.
[24] F. Chen, H.-S. Chu, C.-Y. Soong, W.-M. Yan, J. Power Sources 140 (2004) 243–249.
[25] H.P.L.H. van Bussel, F.G.H. Koene, R.K.A.M. Mallant, J. Power Sources 71 (1998) 218–222.
[26] J.C. Amphlett, R.F. Mann, B.A. Peppley, P.R. Roberge, A. Rodrigues, J. Power Sources 61 (1996) 183–188.
[27] Y. Wang, C.-Y. Wang, Electrochim. Acta 50 (2005) 1307–1315.
[28] D. Natarajan, T.V. Nguyen, J. Electrochem. Soc. 148 (12) (2001) A1324–A1335.
[29] W.-M. Yan, C.-Y. Soong, F. Chen, H.-S. Chu, J. Power Sources 143 (2005) 48–56.
[30] R. Buxbaum, H. Lei, J. Power Sources 123 (2003) 43–47.
[31] B. Emonts, J.B. Hansen, H. Schmidt, T. Grube, B. Höhlein, R. Peters, A. Tschauder, J. Power Sources 86 (2005) 228–236.
[32] M. Sommer, A. Lamm, A. Docter, D. Agar, J. Power Sources 127 (2004) 313–318.
[33] M.J. Khan, M.T. Iqbal, Renew. Energy 30 (2005) 421–439.
[34] M.Y. El-Sharkh, A. Rahman, M.S. Alam, P.C. Byrne, A.A. Sakla, T. Thomas, J. Power Sources 138 (2004) 199–204.
[35] M.Y. El-Sharkh, A. Rahman, M.S. Alam, A.A. Sakla, P.C. Byrne, T. Thomas, IEEE Trans. Power Syst. 19 (4) (2004) 2022–2028.
[36] M. De Francesco, E. Arato, J. Power Sources 108 (2002) 41–52.
[37] J.T. Pukrushpan, H. Peng, A.G. Stefanopoulou, in: Proceedings of the International Mechanical Engineering Congress & Exposition 2002, ASME, 2002, pp. 1–12.
[38] J.T. Pukrushpan, A.G. Stefanopoulou, H. Peng, in: Proceedings of the American Control Conference 2002, 2002, pp. 3117–3122.
[39] S. Caux, J. Lachaize, M. Fadel, P. Shott, L. Nicod, J. Process Control 15 (2005) 481–491.

[40] R.M. Moore, K.H. Hauer, D. Friedman, J. Cunningham, P. Badrinarayanan, S. Ramaswamy, A. Eggert, J. Power Sources 141 (2005) 272–285.
[41] Y. Zhang, M. Ouyang, Q. Lu, J. Luo, X. Li, Appl. Therm. Eng. 24 (2004) 501–513.
[42] H. Weydahl, S.Møller-Holst, T. Burchardt, G. Hagen, in: Proceedings of the 1st European Hydrogen Energy Conference, 2–5 September, 2003.
[43] F. Zenith, H. Weydahl, I.A. Lervik, T. Burchardt, S.Møller-Holst, S. Skogestad, G. Hagen, Proceedings of the 9th Ulm Electrochemical Talks, 16–17 May, 2004.
[44] M. Ciureanu, R. Roberge, J. Phys. Chem. B 105 (2001) 3531–3539.
[45] R.L. Hurt, J.R. MacDonald, Solid State Ionics 20 (1986) 111–124.
[46] A. Lasia, in: B.E. Conway, J.O.M. Bockris, R.E. White (Eds.), Modern Aspects of Electrochemistry, vol. 32, Kluwer Academic/Plenum Publishers, New York, 1999, Chapter 2, pp. 143–247.
[47] V.A. Paganin, C.L.F. Oliveira, E.A. Ticianelli, T.E. Springer, E.R. Gonzalez, Electrochim. Acta 43 (24) (1998) 3761–3766.
[48] J. Larminie, A. Dicks, Fuel cell systems explained, John Wiley & Sons Ltd., Hoboken, 2000, p. 3.
[49] M. Ciureanu, H. Wang, J. Electrochem. Soc. 146 (11) (1999) 4031–4040.
[50] B. Andreaus, A.J. McEvoy, G.G. Scherer, Electrochim. Acta 47 (2002) 2223–2229.
[51] Q. Guo, M. Cayetano, Y. Tsou, E.S. De Castro, R.E. White, J. Electrochem. Soc. 150 (11) (2003) A1440–A1449.
[52] A. Parthasarathy, B. Davé, S. Srinivasan, A.J. Appleby, C.R. Martin, J. Electrochem. Soc. 139 (6) (1992) 1634–1641.
[53] A.J. Bard, L.R. Faulkner, Electrochemical Methods: Fundamentals and Applications, second ed., John Wiley & Sons Inc., Hoboken, 2001, pp. 163–171.